J Nanostruct 10(3): 448-455, Summer 2020

RESEARCH PAPER

# The Effect of rare Earth Lanthanum on the Structure, Microstructure and Magnetic Properties of Magnesium Zinc Based Ferrite Nanoparticles

***Hamed Bahiraei***

*Department of Physics, Faculty of science, Malayer University, Malayer, Iran*

**ARTICLE INFO**

***Article History:***
*Received 14 March 2020*
*Accepted 29 April 2020*
*Published 01 July 2020*

***Keywords:***
*Curie temperature*
*Nanocrystalline material*
*Permeability*
*Spinel structure*

**ABSTRACT**

In this study, a series of $Mg_{0.3}Cu_{0.2}Zn_{0.5}Fe_{2-x}La_xO_4$ ferrite nanoparticles with x= 0 to 0.15, with step 0.015 were synthesized by sol-gel auto combustion method. The effect of rare earth La which was substituted for $Fe^{3+}$, on the structural, microstructure and magnetic properties of prepared samples were investigated. The structural characteristics of samples were studied by X-ray diffraction (XRD) and scanning electron microscopy (SEM). The XRD patterns showed the formation of cubic spinel structure for all samples without any extra peak. The microstructural evaluations showed homogeneous particles and also revealed that their size are about 35 – 50 nm. The magnetic properties of samples were investigated using vibration sample magnetometer (VSM) and Impedance analyzer. Results show that On La substitution, the values of saturation magnetization ($M_S$) were slightly decreased. The real part of permeability as well as Curie temperature were dramatically decreased with increasing x.

**How to cite this article**
*Bahiraei H. The Effect of rare Earth Lanthanum on the Structure, Microstructure and Magnetic Properties of Magnesium Zinc Based Ferrite Nanoparticles. J Nanostruct, 2020; 10(3):448-455. DOI: 10.22052/JNS.2020.03.002*

## INTRODUCTION

In recent years, NiZn-based spinel ferrites have been widely used for production of chip inductor components that are used in visual and audio equipment such as telecommunication devices, liquid crystal TV and computer [1]. MgZn-based spinel ferrites are important magnetic materials that can be replaced instead of NiZn-based ferrites due to thier lowering of magnetostriction constant, environmental considerations and low cost [2].

The properties of spinel ferrite materials are generally governed by the chemical composition and methods followed for preparation. Addition of rare earth (RE) ions to ferrite materials produces a change in their magnetic, electrical as well as structural properties. Many researches have been done to investigate the substitution of rare earth ions such as $Sm^{3+}$, $Gd^{3+}$, $Nd^{3+}$, $Dy^{3+}$, $Y^{3+}$ and $Eu^{3+}$ ions in ferrites. The results show that the addition of small amount of different rare earth ions behave differently depending upon the amount and the type of RE elements used [3-8]. Generally, the enters into the octahedral sites by displacing a proportionate number of $Fe^{3+}$ from octahedral to tetrahedral sites. They have limited solubility in the spinel lattice due to their large ionic radii. Rare earth ions according to their ionic radius can be divided into two categories; close to radius of $Fe^{3+}$ ions and larger than radius of $Fe^{3+}$ ions. The difference in the ionic radii values causes to micro strains. Thus, RE ions can partially occupy the

* *Corresponding Author Email: hamedbahiraei@gmail.com*

octahedral sites as well as form orthoferrite phase ($REFeO_3$) which cause changes in the structural and magnetic behavior of the ferrites and affect domain wall motion resulting in deformation of the spinel structure. They also can influence permeability and resistivity in $MFe_{2-z}RE_zO_4$ ferrites.

The magnetic properties of ferrites are very sensitive to the processing parameters especially preparation method. Sol-gel combustion rote is a promising method for nanostructured of nanostructured ferrite with high surface energy. The nanoscale powders have potential to tailor shrinkage versus temperature behavior [9-15]. In the present work, $Mg_{0.3}Cu_{0.2}Zn_{0.52}La_xFe_{1.98-x}O_{3.99}$ ($0.00 \leq x \leq 0.06$) nanopowders were synthesized via a sol-gel autho combustion method and the structure, microstructure and magnetic properties of prepared nanopowders were studied. After that, the prepared powders were pressed and sintered at 950 °C and the effect of La dopant on their permeability and Curie temperature were measured.

## MATERIALS AND METHOD

$Mg(NO_3)_2.H_2O$, $Cu(NO_3)_2.3H_2O$, $Zn(NO_3)_3.4H_2O$, $Fe(NO_3)_3.9H_2O$, $La(NO_3)_3.6H_2O$, citric acid and ammonium hydroxide were purchased from Merck and used without further purification. The phase formation of samples was identified using X-ray diffraction (XRD; Cu-$K_\alpha$ radiation, λ=1.5418Å). The microstructure was investigated by use a field emission scanning electron microscope (FE-SEM). The magnetic properties were carried out in room temperature using a vibrating sample magnetometer (VSM) device and RF-Impedance analyzer (HP-4991A) in a frequency range of 1 MHz to 80 MHz.

*Synthesis of nanopowders*

Ferrite nanopowders were prepared through nitrate–citrate auto combustion method. Briefly, metal nitrates in stoichiometric ratio were dissolved in deionized water. Then, citric acid solution was added to the mixture and after adjusting the pH value with ammonia to 7, the resultant solution was heated at 80 ºC under constant stirring to transform into a xerogel. During heating the dried gel burnt out in a self-propagating combustion manner to form a fluffy powder. The as-burnt precursor powder was calcined at 600 ºC in air for 2 hours. For measuring permeability the prepared powders granulated using 2wt % PVA and uniaxially pressed at a to form toroid. Finally, the pressed samples were sintered at 900 ºC for 4 hours.

## RESULTS AND DISCUSSION

To investigate the formation of spinel structure of powders the phase analysis was performed using x-ray diffraction technique. Fig. 1 shows

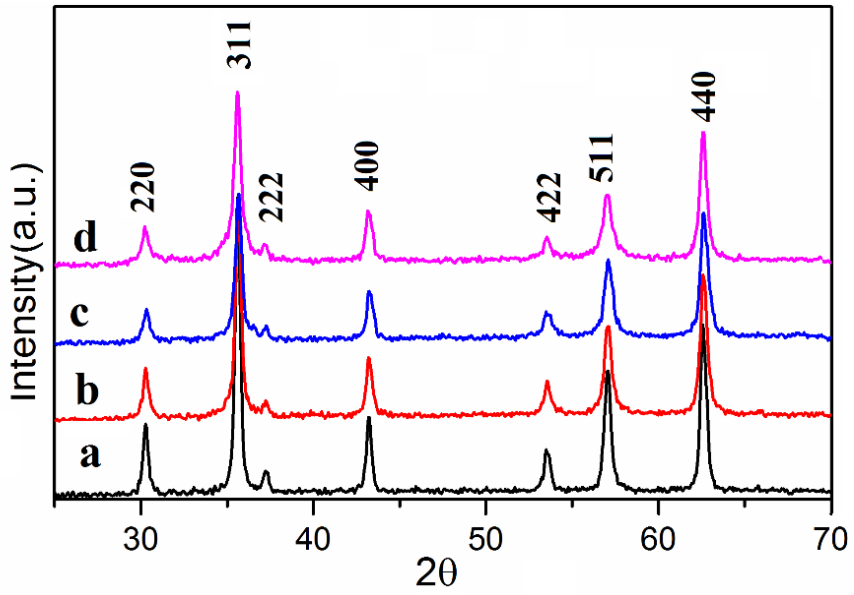


Fig. 1. X-ray diffraction patterns of prepared ferrites with x= 0.00 (a), 0.015 (b), 0.030 (c) and 0.045 (d)

the XRD patterns of the prepared nanopowders. As can be seen, all powders present the main peaks corresponding to a single phase cubic spinel structure with good crystallization that can be indexed using the standard JCPDS card No. 08-0234. The absence of any peak in XRD patterns proves that there is no lanthanum iron oxide, ($LaFeO_3$) phase in all La-substituted ferrites. This indicate that $La^{3+}$ ions may enter the octahedral site and replace the $Fe^{3+}$ ions. Table 1 shows the lattice parameters and crystallite size of the ferrite powders. The average crystallite size (D) of the synthesized compounds is calculated to be 26-37 nm using Scherrer's equation, $D=K\lambda/\beta Cos\theta$, where β is FWHM (width of the observed diffraction peak at its half maximum intensity), λ is the X-ray wavelength ($CuK_\alpha$ radiation, equals to 0.154 nm) and K is the shape factor.

The FE-SEM micrographs of the as-prepared nanopowders are shown in Fig. 2-5. The average particle size of prepared powders is calculated by line intercept technique and presented in

Table 1. Crystallite size, Average particle size of nanopowders, Saturation Magnetization ($M_s$), magnetic moment ($n_B$), Coercivity ($H_c$), permeability (μ′) and Curie temperature ($T_c$) of samples.

| La content (x) | 0.00 | 0.015 | 0.030 | 0.045 |
|---|---|---|---|---|
| Crystal size (nm) | 37 | 26.1 | 26.0 | 25.5 |
| Particle size (nm) | 35 | 46 | 50 | 41 |
| $M_s$ (emu/g) | 37.90 | 31.97 | 29.47 | 25.40 |
| $n_B(\mu_B)$ | 5.2 | 5.125 | 5.05 | 4.975 |
| $H_C$(Oe) | 32 | 26 | 36 | 16 |
| μ′ | 146 | 98 | 72 | 38 |
| $T_C$ (°C) | 136 | 123 | 119 | 116 |

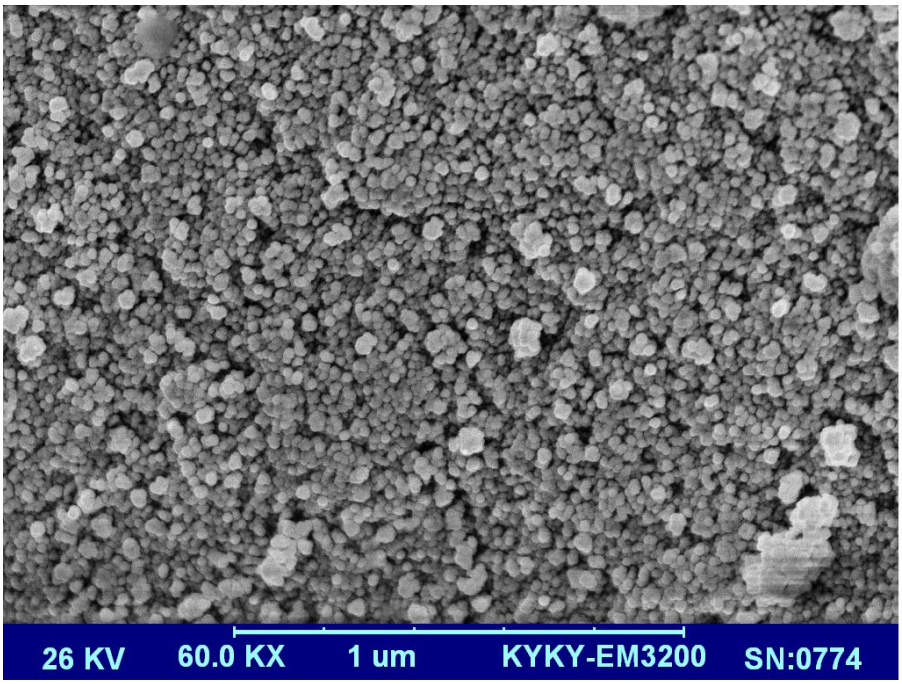


Fig. 2. FE-SEM micrograph of the as-prepared nanopowder with x= 0.00.

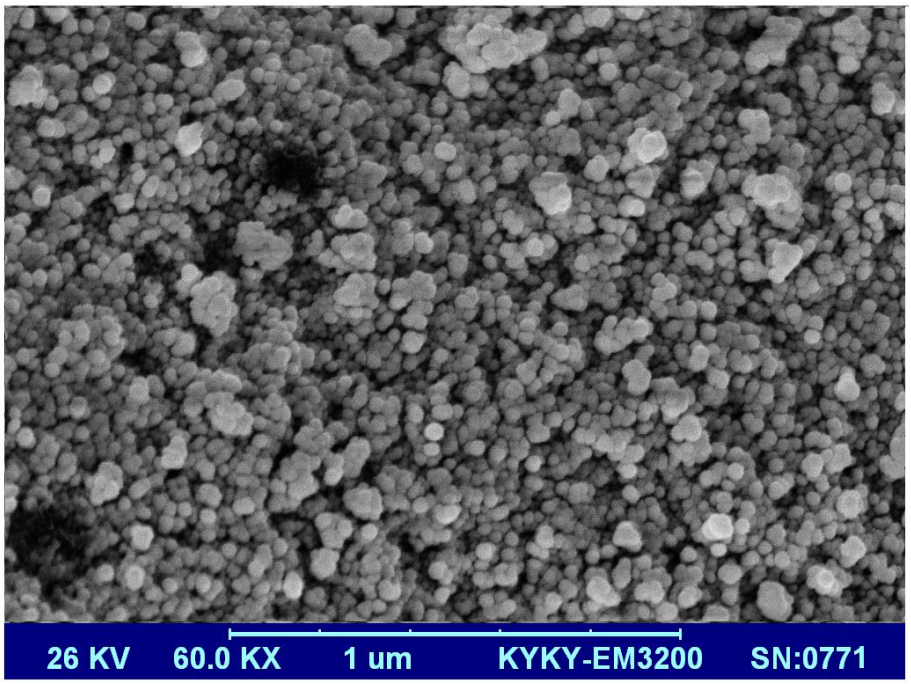


Fig. 3. FE-SEM micrograph of the as-prepared nanopowder with x= 0.015

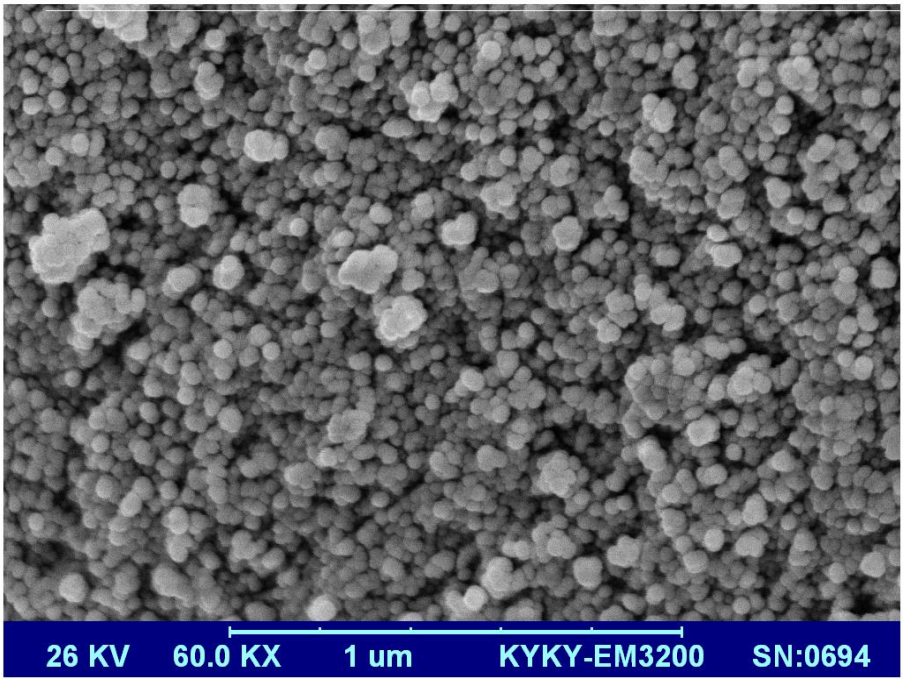


Fig. 4. FE-SEM micrograph of the as-prepared nanopowder with x= 0.030

Table 1. Results reveal the formation of prepared compounds in the form of nanoparticles with the particles size between 35-50 nm. It seems from SEM image that the size of particles increases with La content.

Fig. 6 displays a typical FE-SEM micrographs of

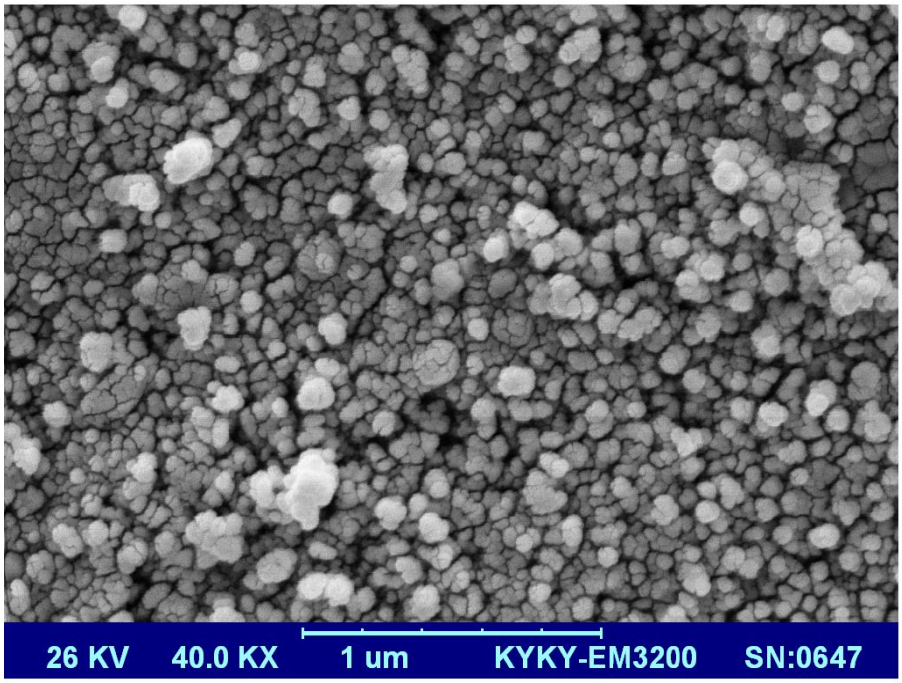


Fig. 5. The FE-SEM micrograph of the as-prepared nanopowder with x= 0.045.

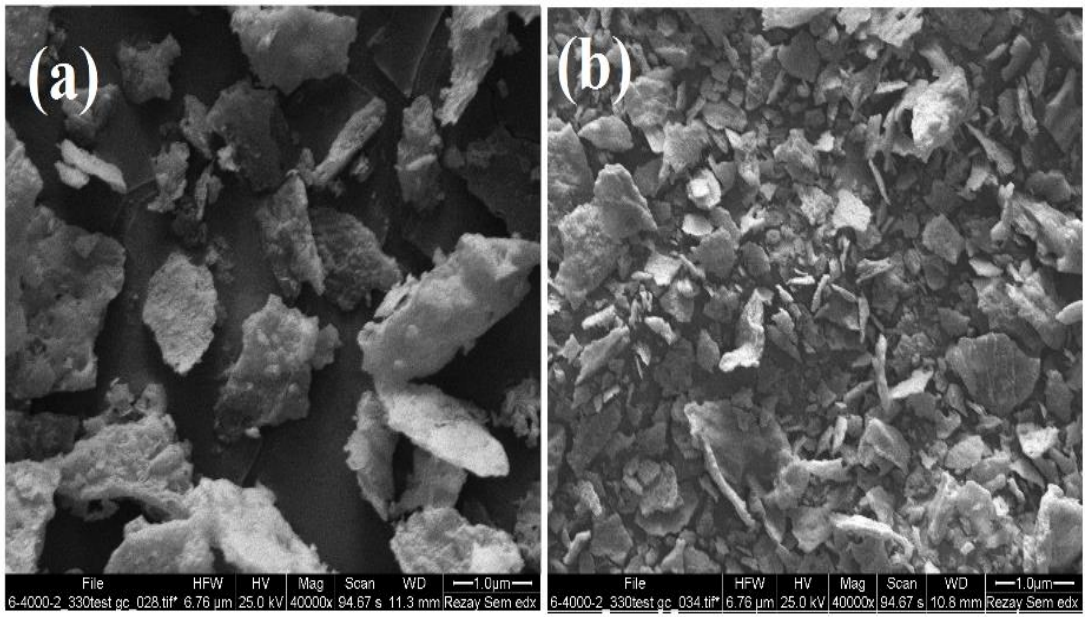


Fig. 6. FE-SEM micrographs of the calcined powders with (a) x= 0.00 and (b) x=0.015.

the nanopowder calcined at 600 C with x=0.00 and 0.015. It is clear that the individual nanoparticles are closely packed to form nano sheets at different sizes. The surface morphology of the different compositions appear to be different from each other.

Fig. 7 shows the magnetic hysteresis curves of the prepared powders measured at room temperature. The low value of coercivity for all the samples shows that the particular sample reveal the soft magnetic action. The saturation magnetization ($M_s$) values are listed in Table 1. It

is seen that $M_s$ continuously decreases with La concentration. This variation could be explained on the basis of tow sub-lattice collinear model suggested by Neel. According to Neel's model the magnetic moment ($n_B$) of ferrite can be calculated using the difference of magnetic moment of B sublattice and A sublattice using the relation [10]:

$$n_B(\mu_B)=M_B-M_A \quad (1)$$

where $M_A$ and $M_B$ are the A and B sublattice magnetic moment in $\mu_B$. Also, the relationship between saturation magnetization ($M_S$) and magnetic moment ($n_B$) is:

$$n_B(\mu_B)= MW* Ms /5585 \quad (2)$$

$M_s$ is the saturation magnetization, MW is the molar weight of compound and $n_B$ is the number of magnetic moment in $\mu_B$.

It is known that in the spinel ferrites $Zn^{2+}$ (0 $\mu_B$) ions occupy A-sites while $Mg^{+}$ (0 $\mu_B$) and $Cu^{2+}$ (+1 $\mu_B$) have considerable B-sites preference [10]. Also, $La^{3+}$ (0 $\mu_B$) ion completely occupy B-site and $Fe^{3+}$ (+5 $\mu_B$) ion can occupy both A and B sites. Thus, cation distribution for $Mg_{0.3}Cu_{0.2}Zn_{0.52}La_xFe_{2-x}O_4$ is assumed to be:

$$(Zn_{0.5}Fe_{0.45})\ [Mg_{0.3}\,Cu_{0.2}La_xFe_{1.5-x}]O_2 \quad (3)$$

Where the brackets () and [] denote to A- and B-sites, respectively.

Table 1 shows the calculated values for the number of magnetic moments ($n_B$). According to the above relations, as $La^{3+}$ has negligible magnetic moment, which does not take part in the exchange interaction to the nearest neighbour ions, the magnetization of B-sites decreases with La content and so the total saturation magnetization decreases.

To investigate the applicability of the prepared powders, they were pressed in toroidal shape and sintered at 950 °C. The magnetic permeability ($\mu_i$) and Curie temperature of sintered samples were measured by using impedance analyzer. Results are listed in Table 1. Fig. 8 displays magnetic permeability of samples as a function of frequency. It is seen the samples with La have lower values of permeability ($\mu_i$) than that of undoped sample (at 1 MHz) and permeability decreases with increasing La content. According to Table 1, results show that $\mu_i$ follows the same behavior as that of $M_s$ where a maximum is noticed at x=0.00. On substitution of $La^{3+}$ ion Curie temperature is found to be decreased because, $La^{3+}$ ion that occupy octahedral site can make La–Fe interaction and this interaction is weaker than Fe–Fe interaction in octahedral site. The dilution of interaction in octahedral sites is responsible for the decreases of

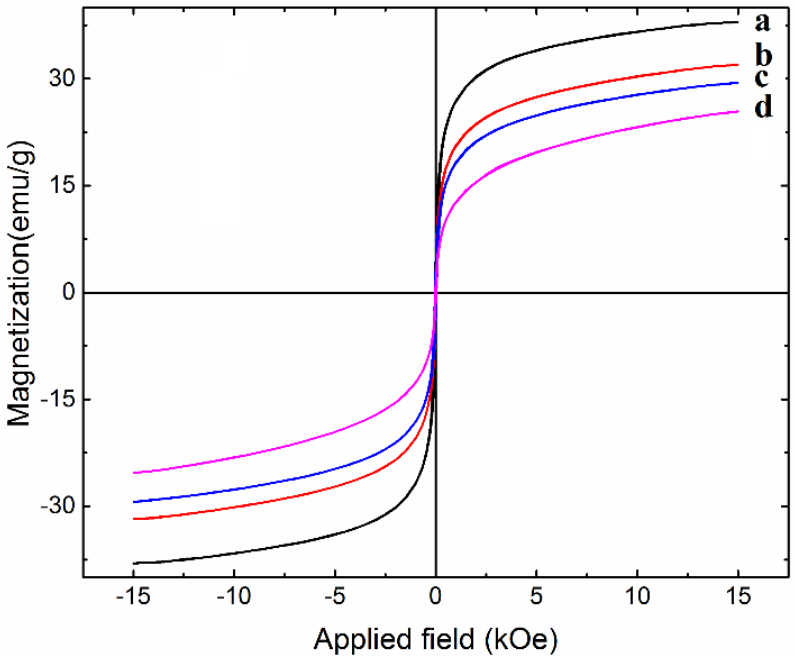


Fig. 7. Hysteresis curves of prepared nanopowder with x= (a) 0.00, (b) 0.015, (c) 0.030 and (d) 0.045

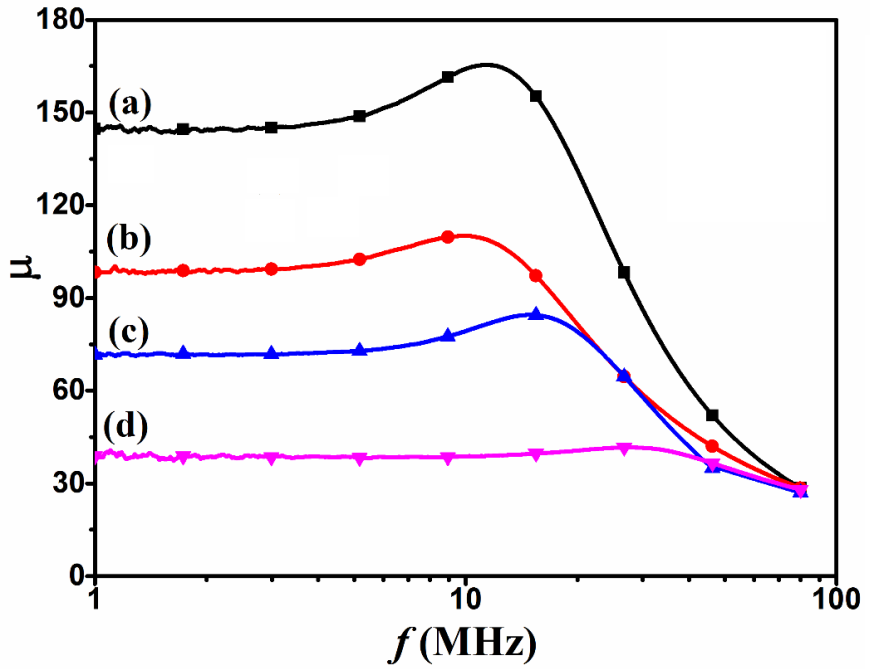


Fig. 8. Frequency dependency of initial permeability for sintered samples with x= (a) 0.00, (b) 0.015, (c) 0.030 and (d) 0.045

Curie temperature.

## CONCLUSION

A series of $Mg_{0.3}Cu_{0.2}Zn_{0.5}Fe_{2-x}La_xO_4$ ferrites nanopowders with x=0.00, 0.015, 0.030 and 0.045 have been prepared through the combustion method. The effect of La ion (x) on the structural, microstructural and magnetic propeties of samples was investigated, and the following results have been obtained. The X-ray diffraction patterns exhibited the formation of cubic spinel structure. The morphology of powders characturized by SEM is found to contain homogeneous nanoparticles 35–50 nm. Results show that $La^{3+}$ ion has significantly effect on the magnetic properties of prepared samples. The saturation magnetization of nanopowders was found to be slightly decreased with x. Furthermore, permeability and Curie temperature was found to be decreased with x.

## CONFLICT OF INTEREST

The authors declare that there is no conflict of interests regarding the publication of this manuscript.

## REFERENCES

1. Varalaxmi N, Sivakumar KV. Structural, magnetic, DC–AC electrical conductivities and thermo electric studies of MgCuZn Ferrites for microinductor applications. Materials Science and Engineering: C. 2013;33(1):145-152.
2. Bhosale DN, Choudhari ND, Sawant SR, Kale RD, Bakare PP. Synthesis of high permeability Cu-Mg-Zn ferrites using oxalate precursors. IEEE Trans Magn. 1998;34(2):535-541.
3. Asif Iqbal M, Misbah ul I, Ali I, Khan HM, Mustafa G, Ali I. Study of electrical transport properties of $Eu^{+3}$substituted MnZn-ferrites synthesized by co-precipitation technique. Ceram Int. 2013;39(2):1539-1545.
4. Gadkari AB, Shinde TJ, Vasambekar PN. Structural analysis of $Y^{3+}$-doped Mg–Cd ferrites prepared by oxalate co-precipitation method. Mater Chem Phys. 2009;114(2-3):505-510.
5. Kambale RC, Song KM, Koo YS, Hur N. Low temperature synthesis of nanocrystalline $Dy^{3+}$ doped cobalt ferrite: Structural and magnetic properties. J Appl Phys. 2011;110(5):053910.
6. Zhao L, Yang H, Zhao X, Yu L, Cui Y, Feng S. Magnetic properties of $CoFe_2O_4$ ferrite doped with rare earth ion. Mater Lett. 2006;60(1):1-6.
7. Shinde TJ, Gadkari AB, Vasambekar PN. Influence of $Nd^{3+}$ substitution on structural, electrical and magnetic properties of nanocrystalline nickel ferrites. J Alloys Compd. 2012;513:80-85.

8. Chand J, Kumar G, Kumar P, Sharma SK, Knobel M, Singh M. Effect of $Gd^{3+}$ doping on magnetic, electric and dielectric properties of $MgGd_xFe_{2-x}O_4$ ferrites processed by solid state reaction technique. J Alloys Compd. 2011;509(40):9638-9644.
9. Bahiraei H, Shoushtari MZ, Gheisari K, Ong CK. The effect of sintering temperature on the electromagnetic properties of nanocrystalline MgCuZn ferrite prepared by sol–gel auto combustion method. Mater Lett. 2014;122:129-132.
10. Bahiraei H, Shoushtari MZ, Gheisari K, Ong CK. The effect of non-magnetic $Al^{3+}$ ions on the structure and electromagnetic properties of MgCuZn ferrite. J Magn Magn Mater. 2014;371:29-34.
11. Ahmadian-Fard-Fini S, Salavati-Niasari M, Ghanbari D. Hydrothermal green synthesis of magnetic $Fe_3O_4$–carbon dots by lemon and grape fruit extracts and as a photoluminescence sensor for detecting of E. coli bacteria. Spectrochim Acta A. 2018;203:481-493.
12. Ahmadian-Fard-Fini S, Ghanbari D, Amiri O, Salavati-Niasari M. Electro-spinning of cellulose acetate nanofibers/Fe carbon dot as photoluminescence sensor for mercury (II) and lead (II) ions, Carbohydr Polym. , 2020;229, 115428.
13. Moradi B, Nabiyouni G, Ghanbari D. Rapid photo-degradation of toxic dye pollutants: green synthesis of mono-disperse $Fe_3O_4$–$CeO_2$ nanocomposites in the presence of lemon extract. J Mater Sci: Mater Electron., 2018; 29 (13), 11065-11080.
14. Etminan M, Nabiyouni G, Ghanbari D. Preparation of tin ferrite–tin oxide by hydrothermal, precipitation and auto-combustion: photo-catalyst and magnetic nanocomposites for degradation of toxic azo-dyes. J Mater Sci: Mater Electron.. 2018;29: 1766–1776.
15. Ahmadian-Fard-Fini S, Ghanbari D, Salavati-Niasari M. Photoluminescence carbon dot as a sensor for detecting of Pseudomonas aeruginosa bacteria: Hydrothermal synthesis of magnetic hollow $NiFe_2O_4$-carbon dots nanocomposite material. Compos Part B-Eng 2019;161:564-577.